



## Flaw classification in bonded joints using multivariate statistical analysis and artificial intelligence

Carlos Tais<sup>a,d</sup>, Juan M. Fontana<sup>a,c</sup> , Leonardo Molisani<sup>a,c</sup>, Ronald O'Brien<sup>a</sup>, Yolanda Ballesteros<sup>b</sup>, Raquel Caro Carretero<sup>b</sup> , Juan C. del Real-Romero<sup>b,\*</sup> 

<sup>a</sup> Group of Acoustics and Vibrations (GAV), National University of Río Cuarto (UNRC), National Road N° 36 Km 601, 5800, Río Cuarto, Argentina

<sup>b</sup> Mechanical Engineering Department, Institute for Research in Technology, Comillas Pontifical University of Madrid, Alberto Aguilera, 23, 28015, Madrid, Spain

<sup>c</sup> Institute of Development for Agro-industrial and Health (IDAS), UNRC-CONICET, National Road N° 36 Km 601, 5800, Río Cuarto, Argentina

<sup>d</sup> National Technological University, Regional Faculty Villa María, Av. University 450 CP 5900 Villa María, Córdoba, Argentina

### ARTICLE INFO

#### Keywords:

Artificial intelligent  
Bonded joints  
Flaw detection  
Neural networks  
Acoustic signals

### ABSTRACT

Adhesives play an important role in multiple industries, offering versatile bonding solutions for diverse applications. However, their incorporation in structures where safety is critical has been met with hesitation due to potential degradation risks. Addressing this concern, this study introduces the preliminary assessment of a pattern recognition method aimed at automatically identifying damage in adhesive joints through acoustic signal analysis. This method was tested on experimental samples consisting of aluminum substrates bonded with an acrylic adhesive. Artificially generated defects on the samples was related to the percentage of bonded surface. Damaged samples contained either 25 %, 50 %, or 75 % of bonded surface, whereas healthy samples contained 100 % of bonded surface. Experiments involved applying an impulsive load at one end of the sample and recording the acoustic signal emitted in response to the load using a microphone located at the opposite end. Two classification algorithms were evaluated for discriminating the amount of damage of the samples. First, a multivariate statistical analysis extracted the fundamental frequencies from the acoustic signals to create a model that achieved 95 % of classification accuracy. Second, an Artificial Neural Network (ANN) model was trained and validated with features extracted from the sound pressure level (SPL) signal obtaining an average accuracy of 97.1 % for a 9-fold cross-validation. The results indicate that there is potential for further exploration of the proposed approach, leading to the development of a robust system capable of automatically detecting damage in bonded joints. Future work will explore the performance of the classification techniques for detecting other types of defects related to the lack of adhesion and inadequate curing times.

### 1. Introduction

Structural adhesives represent an increasingly prevalent alternative to traditional joining techniques such as welding, screws, or rivets. This shift is particularly evident in industries demanding high-performance, lightweight structures like aerospace, automotive, and shipbuilding, in household appliances and metal constructions [1]. The efficacy of adhesive bonds lies not only in their ability to enhance efficiency and flexibility in production processes but also in their capacity to join disparate materials, yielding numerous benefits. These advantages include, but are not limited to, significant weight reduction, enhanced fatigue resistance, and superior electrical and thermal insulation [2].

One of the fundamental merits of adhesive joints over conventional mechanical joints is their non-distorting nature, which contrasts sharply with the effects observed in weld bonding or joints involving mechanical elements [3–7].

Adhesive bonds provide continuous joints, rather than point-based ones like spot welding, thereby ensuring an even stress distribution and heightened rigidity. Well-designed adhesive joints also excel in energy absorption and demonstrate effective vibration and noise damping properties.

The term “structural” encompasses a broad array of adhesives like epoxy, cyanoacrylates, acrylics, and polyurethanes. Epoxies, in particular, have gained wide traction, especially in the aerospace and

This article is part of a special issue entitled: Euradh 2023 Special Issue published in International Journal of Adhesion and Adhesives.

\* Corresponding author.

E-mail addresses: [gav@ing.unrc.edu.ar](mailto:gav@ing.unrc.edu.ar) (C. Tais), [delreal@comillas.edu](mailto:delreal@comillas.edu) (J.C. del Real-Romero).

<https://doi.org/10.1016/j.ijadhadh.2025.104032>

Received 17 July 2024; Received in revised form 21 March 2025; Accepted 7 April 2025

Available online 12 April 2025

0143-7496/© 2025 Elsevier Ltd. All rights reserved, including those for text and data mining, AI training, and similar technologies.

automotive industries [8].

A family of adhesives such as tough acrylic adhesives, have not been fully utilized or thoroughly studied in bonding structures composed of aluminum-based alloy components, despite their significant potential for application. These adhesives possess characteristics that make them particularly useful for joining metallic materials; their ability to cure at room temperature, their high curing speed, high resistance to fracture and peeling, and their ability to produce satisfactory bonds on surfaces with minimal surface preparation suggest that these adhesives could be a solution for many bonding processes [9–11].

Despite these advances, several challenges and limitations persist, particularly regarding curing times and the susceptibility of adhesive bonds to peeling stresses. This latter aspect notably constrains the design of joints. Defects primarily occur during the application and curing process, weakening the adhesive joint. These defects can originate either at the adhesive-substrate interface or within the adhesive itself, often exacerbated by inadequate substrate surface preparation. Recognizing and addressing these challenges is crucial, as any surface contamination, such as grease, can critically undermine the adhesion process [12].

In response to these challenges, several non-destructive testing (NDT) methods has been developed and refined. Techniques such as visual inspection, microscopy (light and electron), X-ray, C-Scan, IR thermography, and IR radiometry have become instrumental in monitoring potential defects and assessing the integrity of adhesive joints [13,14]. Acoustic-ultrasonic wave methods, including pulse-echo, transmission techniques, and guided wave-based methods, offer detailed insights into the material's structural integrity and properties [15]. Moreover, the recent integration of artificial intelligence tools has revolutionized NDT by recognizing and classifying damage patterns in adhesive joints. Pattern recognition methods, particularly those based on machine learning algorithms, can be trained using labeled data, where examples of both healthy and damaged conditions are provided, allowing the algorithm to learn the distinguishing features of each [16–19]. This enables the algorithm to generalize its knowledge to new, unseen data and adapt to changing conditions without manual intervention. The main advantage of pattern recognition methods lies in their ability to efficiently analyze large and diverse datasets to identify subtle patterns associated with different types of damage. Chiang et al. [20]; Chiang and Russell [21,22]; Li et al. [17]; Jasiūnienė et al. [16]; Ramalho et al. [18]; Malinowski et al. [23].

Artificial Neural Networks (ANNs) are computational systems inspired by the structure and functioning of the human brain [24]. They are composed of elementary units called neurons that are organized in a layered architecture that includes an input layer, one or more hidden layers, and an output layer. Each neuron receives multiple input signals, which are linearly combined through assigned weights and then transformed by applying a non-linear activation function (such as the sigmoid, the rectified linear unit function ReLU, or tanh) to produce an output. This characteristic enables ANNs to model complex, non-linear relationships among variables, approximating complicated functions through data-driven learning. Generally, ANNs are trained using backpropagation algorithms that iteratively adjust the weights to minimize an error function [25]. During the training process, data is passed through the neurons from the input to the output, and the network's output is compared to known target values. The goal is to reduce the error between the processed output and these target values. This error is quantified through a continuously differentiable performance function that depends on all the weights in the network. By iteratively adjusting these weights via backpropagation, the network learns to approximate the desired function. The quality of a trained ANN is evaluated through metrics such as accuracy, sensitivity, specificity, and loss, complemented by cross-validation techniques and confusion matrix analysis, ensuring its capacity to generalize.

ANNs have demonstrated their versatility by being applied in various fields. For example, in image recognition, these networks have enabled significant advances in identifying and classifying visual patterns,

playing a fundamental role in computer vision applications [26]. In natural language processing, ANNs facilitate the semantic and syntactic analysis of texts, enhancing tasks such as machine translation and content generation [27]. In fault detection, ANNs are used to identify anomalies in vibrational behavior of rotating machinery, which helps prevent critical failures [28]. ANNs have also been integrated into non-destructive analysis (NDA) techniques for assessing structural integrity by interpreting signals from various sensors [29–31]. In the specific field of damage detection in adhesive joints, ANNs have been applied to recognize degradation patterns and classify the state of adhesion, thereby facilitating the identification of defects in the joint [18,32,33]. Another approach is to integrate ANNs with acoustic signals derived from the impulse response of adhesively bonded samples. This integration represents a viable and feasible research avenue for non-intrusive damage assessment in adhesive joints, as it enables the extraction and analysis of distinctive acoustic features and patterns indicative of joint integrity.

Linear Discriminant Analysis (LDA), also known as Fisher Discriminant Analysis, is a classical statistical technique used for dimensionality reduction and classification. LDA operates by finding a linear combination of features that best separates multiple classes. It does so by maximizing the ratio of the between-class variance to the within-class variance under the assumption that data from each class are drawn from a Gaussian distribution with identical covariance matrices. This approach yields an analytically derived discriminant function that is both computationally efficient and highly interpretable. In the field of NDT, LDA has been applied in combination with a machine learning algorithm to evaluate the integrity of adhesively bonded joints. For instance, LDA has been used to explore the importance of various feature subsets extracted from ultrasonic signals to distinguish between healthy joints and those exhibiting adhesive failures [34,35].

Both LDA and ANN represent viable research avenues for NDT applications. LDA are based on clear statistical assumptions that offers transparent decision boundaries and provides a straightforward and efficient solution when its underlying assumptions are met. Artificial Neural Networks (ANNs) are flexible, non-parametric models capable of capturing complex, non-linear relationships in large, high-dimensional datasets at the expense of interpretability. Thus, these methods present unique advantages and limitations that warrant further investigation.

These innovations collectively highlight the dynamic and rapidly evolving field of adhesive technology and nondestructive evaluation, underscoring the critical role of advanced computational techniques in enhancing structural integrity and performance in diverse industrial applications. Inspired by these advances, this study introduces the preliminary assessment of a pattern recognition technique designed to automatically detect damage in adhesive joints through acoustic signal analysis. Two classification algorithms (FDA and ANN) were tested on experimental samples that had artificially generated defects, thus achieving different percentages of bonded surface (25, 50, 75 and 100 %).

The remainder of this paper is organized as follows: Section 2 describes the experimental setup, detailing the materials, specimen fabrication, and acoustic signal acquisition process. Section 3 presents the data processing methodology, including feature extraction and classification techniques based on both Linear Discriminant Analysis (LDA) and Artificial Neural Networks (ANNs). Section 4 discusses the results obtained from the classification models, comparing their performance in detecting damage in adhesively bonded joints. Finally, Section 5 summarizes the main findings of this study and outlines potential directions for future research in non-destructive evaluation methods for adhesive joints.

## 2. Experimental procedure

### 2.1. Materials

In the present experiments, rectangular substrates of wrought aluminum EN AW 6082 substrates were used. The nominal size was 25 mm wide, 150 mm long and 4 mm thick. The adhesive chosen was Loctite Hysol H4800 Speedbonder, which is a two-component toughened acrylic adhesive, supplied by Henkel Iberica (Madrid, Spain). The components were mixed in a 10:1 vol ratio using a Sulzer Mixpac DM 400 Cartridge Gun and a disposable Static Elix mixer F-system syringe.

### 2.2. Specimen fabrication

Forty bonded specimens were prepared from 80 aluminum substrates. Prior to applying the adhesive, the bonding area of each sample was grit blasted with aluminum oxide of 0,3 mm and thoroughly cleaned using methyl ethyl ketone (MEK) solvent and lanolin-free tissues. The substrates were bonded together with an overlap length of 30 mm and each specimen was subsequently marked on its edges to denote the end of the bond region. The thickness of the adhesive to be achieved was determined as 1 mm.

To generate faults within the bonded joints, varying amounts of adhesive, i.e. 100 %, 75 %, 50 %, and 25 % of bonding of the total bonded surface, were applied to the aluminum adherent pairs (Fig. 1). The partial adhesion was achieved using Teflon inserts placed on the center of the bonding surface of each specimen before applying adhesive.

During bonding, the single-lap shear specimens were kept in a jig to obtain a uniform bond line. The samples were allowed to cure for 24 h in a desiccator before Teflon inserts were removed.

Four groups of ten specimens were manufactured for failure condition (G100, G75, G50 and G25 contain specimens with 100 %, 75 % 50 % and 25 % of bonding of the total bonded surface, respectively). The following variables were measured from each specimen: adhesive mass, adhesion width, overlap length, adhesive thickness, and length, width, thickness and weight of the aluminum adherents. The average value and standard deviation across all specimens is reported in Table 1. The greatest variability was found in the adhesive weight ( $0.72 \pm 0.22$  g) because the specimens with the highest percentage of damage (G25) have a much lower adhesive weight than the specimens in G100.

### 2.3. Acoustic testing. Sound pressure level (SPL)

To obtain the sound pressure level (SPL) signal, each specimen was

**Table 1**  
Specimens dimensions.

Aluminum Adherends	Length [mm]	Width [mm]	Thickness (mm)	Weight (g)
ENAW 6082 T6	$150.9 \pm 0.1$	$25.2 \pm 0.2$	$4.06 \pm 0.02$	$41.6 \pm 0.2$
Adhesive Joints	Overlap length (mm)	Adhesion width (mm)	Adhesive thickness (mm)	Adhesive weight (g)
	$31.00 \pm 0.30$	$25.24 \pm 0.02$	$1.05 \pm 0.10$	$0.72 \pm 0.22$
Specimens Groups	G100	G75	G50	G25
Bonded Surface	100 %	75 %	50 %	25 %
No. of specimens	10	10	10	10

mounted on a universal support frame composed of a rigid structure and nylon strings, ensuring free-free boundary conditions at its ends (Fig. 2). The transversal strings supporting the specimen were positioned 60.4 mm from each end, coinciding with the nodes (zero displacement points) of the first oscillation mode.

#### 2.3.1. Signal acquisition

A light impact was manually applied to one end of the specimen using a rigid impact rod, consisting of a 90 mm long machined cylindrical steel piece with a spherical tip to concentrate its mass [36]. The impact was applied 30.2 mm from the edge along the longitudinal symmetry axis to minimize torsional vibrations [36]. This procedure was carefully controlled to ensure minimal contact time between the impact rod and the specimen. In all cases, the applied impact was strong enough to exceed the microphone's trigger threshold (0.02 V) while avoiding excessive force that could displace the specimen from its support points.

The vibrations induced by this external excitation generated acoustic pressure fluctuations, which were captured by a high-sensitivity microphone (model FOG-800, GTC) positioned at the opposite end of the specimen. This omnidirectional microphone converts acoustic waves into electrical signals, which were then processed using a data acquisition card connected to a personal computer. The microphone features a sensitivity of 125 Pa/mV, an output impedance of 2.2  $\Omega$ , and a flat frequency response in the 100 Hz to 16 kHz range. Since the analyzed frequency range lies within this range, the obtained frequency spectra are highly reliable. To ensure measurement accuracy, a calibration procedure was performed using the intercomparison method, where

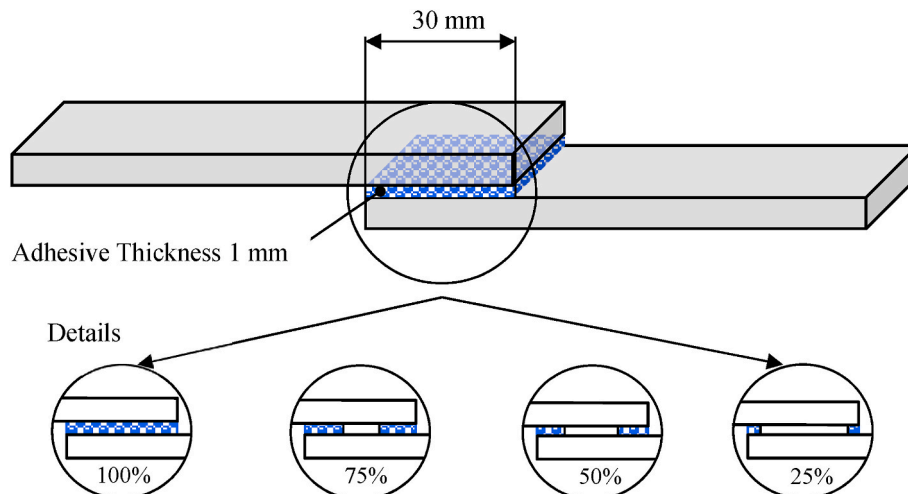


**Fig. 1.** Schematic illustration of four sets of bonded joints with varying degrees of bonding.



Fig. 2. Sound pressure level measurement system. (1) Universal wire support (2) Impact rod (3) USB microphone (4) Laptop with dedicated software.

results from three different microphones were compared. A total of 20 measurements were taken with each microphone, yielding a relative error of less than 0.1 %.

The acoustic signal recording began when the microphone's trigger threshold voltage (0.02 V) was exceeded following the impact. The recording duration was set to 0.5 s, ensuring sufficient signal acquisition to capture a complete frequency response within the desired range.

### 2.3.2. Sound pressure level calculation

The acquired signal was analyzed using custom software, and the SPL was determined as follows:

$$SPL(\omega) = 10 \log_{10} \left( \frac{P_{rms}^2}{P_{ref}^2} \right) \quad (1)$$

where  $P_{ref}$  is the reference sound pressure of 20  $\mu\text{Pa}$ , a conventionally defined value based on human hearing physiology, used to standardize SPL measurements [37,38]. The term  $P_{rms}^2$  represents the root mean square of the acoustic pressure signal and was calculated as:

$$P_{rms}^2 = \frac{1}{N} \sum_{i=1}^N |P(\omega_i)|^2 \quad (2)$$

where  $P(\omega_i)$  are the spectral coefficients obtained from the Discrete Fourier Transform (DFT) of the time domain signal,  $|P(\omega_i)|^2$  represents the spectral energy density at each frequency  $\omega_i$  and  $N$  is the total number of samples in 0.5 s of signal recording.

A sampling frequency of 16 kHz was used, resulting in 8000 samples for the time domain signal. However, as the DFT produces a symmetric spectrum, only the first half of the coefficients were considered, meaning that  $N = 4000$  frequency points were used. Furthermore, frequency components below 100 Hz were discarded to comply with the microphone's valid frequency response, leading to a refined dataset of  $N = 3,951$  samples for SPL computation.

### 2.3.3. Signal normalization

Variations in the magnitude of the applied impact force affect the overall amplitude of the acquired signal but do not influence the resonant frequency values. Since the impact rod was not instrumented to measure force and ensure consistency across tests, normalization was applied to make the SPL results independent of the excitation magnitude.

For this purpose, SPL values were normalized relative to the maximum SPL recorded in the first experiment with an undamaged specimen. The normalization for the  $i$ -th measurement was defined as:

$$\overline{SPL}_i = \frac{SPL_i}{\max(SPL_H)} \quad (3)$$

where  $\overline{SPL}_i$  is the normalized sound pressure level for the  $i$ -th test,  $SPL_i$  is the measured sound pressure level and  $\max(SPL_H)$  is the maximum SPL value obtained from tests on the healthy (undamaged) specimen. This normalization ensures that all SPL measurements are relative to a

consistent reference, reducing variability caused by differences in impact force while preserving the integrity of the frequency-based analysis.

### 2.3.4. Data set

A total of 40 specimens, divided into four groups of ten specimens each (G100, G75, G50, and G25), were analyzed. Each specimen underwent 20 tests, resulting in a total of 800 tests. In each test, the resonance frequencies, identified as the frequencies with the highest SPL values, were determined.

Each test revealed six distinct resonant frequencies within the analyzed frequency range. Fig. 3 illustrate the vibration spectra of the 10 specimens from groups G100, G75, G50, and G25, respectively, highlighting these six resonant frequencies. The variations observed among these characteristic frequencies can be attributed to differences in mass, substrate dimensions, and adhesive volume applied. These variations reflect the inherent discrepancies in industrial bonding techniques but do not compromise the integrity of the adhesive joint.

Table 2 summarizes the amplitude and average standard deviation values calculated from the 200 tests conducted for each adhesion group. Variations in the amplitude of resonance peaks do not affect the classification process, as the primary focus of the analysis is the shift in resonance frequency values. Specimens with intentionally induced adhesion defects (G75, G50, and G25) exhibit distinct frequency spectra compared to the intact specimens (G100). This study seeks to determine whether these frequency shifts result from variations in mass, dimensions, or adhesive thickness—as observed in G100—or if they are indicative of bonding defects, as seen in G75, G50, and G25.

## 3. Data processing

### 3.1. Multivariate statistical analysis

Discriminant analysis is a statistical technique widely used for classifying objects or cases into predefined groups by identifying predictor variables that effectively differentiate among these groups. It is especially useful in situations where we need to distinguish between categories while keeping things as clear and structured as possible. One of its main strengths is that it does not just help with classification. It also reveals which variables play the biggest role in making those distinctions, making it a valuable tool for both prediction and understanding patterns in data. Linear Discriminant Analysis (LDA), one of the most well-known versions, works by transforming data in a way that enhances class separation [39,40]. However, discriminant analysis is not just limited to linear methods. More advanced versions, like Quadratic Discriminant Analysis and Kernel Discriminant Analysis, handle more complex patterns, making them useful for more intricate classification tasks [41,42].

The mathematical basis of discriminant analysis involves deriving discriminant functions from independent variables, which in this study correspond to natural frequencies obtained through SPL tests. These functions establish a decision rule by computing discriminant scores,

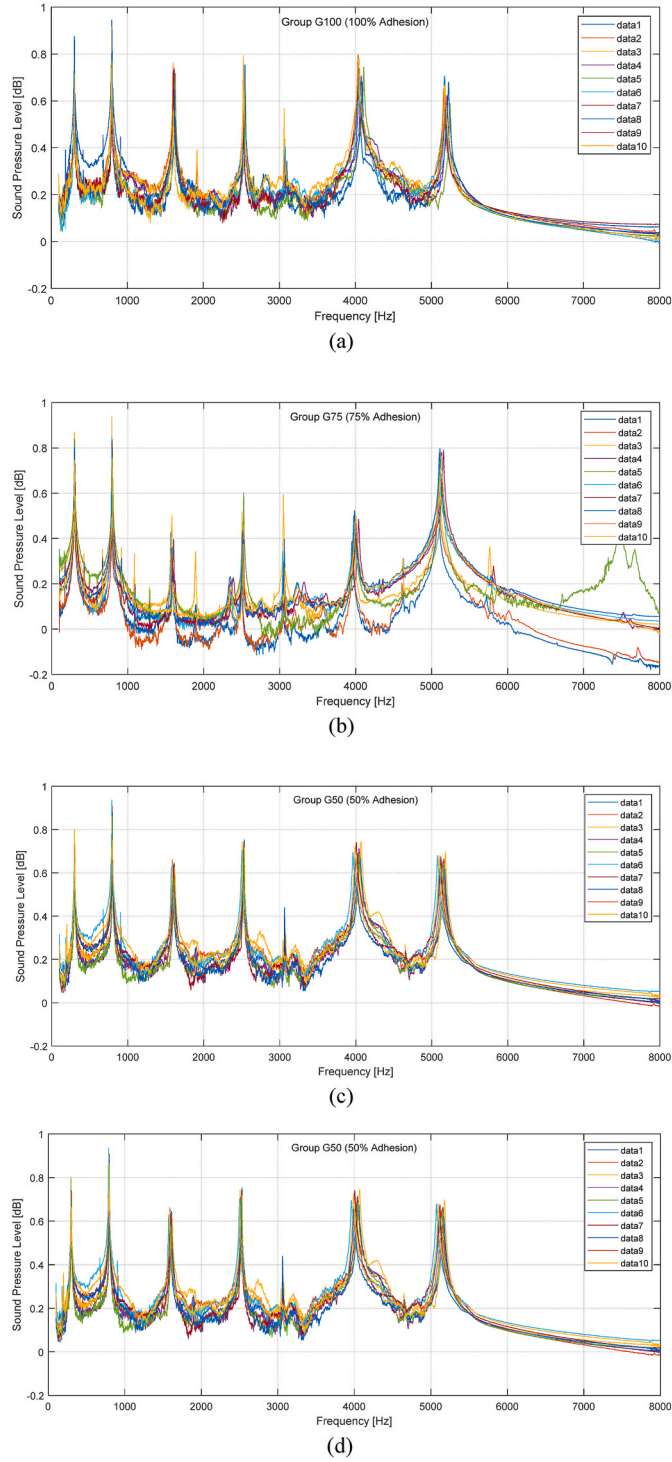


**Fig. 3.** Vibration spectra of the 10 specimens from (a) group G100 (100 % adhesion) (b) group G75 (75 % adhesion) (c) group G50 (50 % adhesion) (d) group G25 (25 % adhesion).

which are subsequently compared across predefined groups to determine the most probable classification for each specimen. These functions are used to classify each specimen into a specific group according to the bonded area percentage of the specimen. By leveraging multivariate statistical techniques, discriminant analysis enhances classification accuracy and robustness, making it a valuable tool in predictive modeling and pattern recognition. The general linear discriminant function is expressed as follows:

$$F_{dis} = B_0 + B_1F_1 + B_2F_2 + B_3F_3 + B_4F_4 + B_5F_5 + B_6F_6 \quad (4)$$

where  $F_n$  represents the independent variables corresponding to vibrational frequencies obtained from SPL testing;  $F_{dis}$  denotes the dependent variable representing the discriminant score used for specimen classification;  $B_0$  is a intercept constant of the discriminant function and  $B_i$  denotes the coefficients calculated through multivariate analysis, optimized to maximize separation among functions corresponding to each group (G100 to G25).

Each tested specimen is evaluated using the four linear discriminant functions derived via Fisher's linear discriminant method (LDA). The specimen is classified into the group whose corresponding discriminant function yields the highest value. Statistical evaluation was performed using IBM SPSS Statistics for Windows, Version 28.0 (IBM Corp., Armonk, NY, USA).

### 3.2. Artificial Neural Network classification model

#### 3.2.1. SPL signal preprocessing

The analysis of the spectral components of the resulting SPL from each test allows determining the characteristic values of the first six natural frequencies of the different specimens based on the means of the 20 tests conducted on each sample (Fig. 3). The variability of the results is observed due to inherent issues in the test itself. Therefore, with the aim of analyzing more homogeneous data and ensuring that the variation is primarily attributed to differences in the adhesion percentage, it is proposed to eliminate the specimen that shows the highest dispersion in the values of the characteristic frequencies compared to the mean ( $\bar{x}$ ) of all tests for each type of defect. Thus, the standard deviation ( $\sigma$ ) of the means of the ten specimens is calculated, and based on these, the data from the specimen whose means of each characteristic frequency fall outside the range  $\bar{x} \pm \sigma$  were excluded from the analysis. This selection was performed for each group of specimens.

For example, in the G100, the specimen 5 exhibits values of the mean of the six frequencies with the highest dispersion relative to the proposed range (Table 3). Thus, specimen 5 with its 20 tests was discarded, and the remaining nine were retained for processing and subsequent classification. In the case of specimens of G25, the same analysis indicates that specimen 10 shows the greatest dispersion resulting in its exclusion. Finally, for specimens of G75 and G50, specimens 1 and 6 were discarded following the same criterion, respectively.

#### 3.2.2. Signal denoising and compression

Prior to processing the data using the neural network algorithm, it is necessary to adapt them in terms of their quality and quantity. The test results contain a level of noise originated from various factors as machinery, ventilation systems, or human activity, so its attenuation or elimination is necessary [43]. With this goal, the Singular Value Decomposition (SVD) technique proposed by [44] was employed, which involves eliminating the content of uncorrelated information while retaining the relevant characteristics of the signal. This procedure is achieved by appropriately selecting the singular values of the Hankel matrix and discarding those below a certain threshold level.

To ensure adequate representation of the system's dynamics, the number of singular values selected for analysis should be greater than twice the number of distinct modes identified in the original sound pressure level (SPL) data within the frequency range of interest [44]. Although 15 singular values were estimated to be sufficient based on this criterion, the 30 largest eigenvalues were chosen for the present investigation. The distribution of normalized eigenvalues for trial 2 of healthy specimen 5 is presented in Fig. 4. A rapid decrease in magnitude is observed for the first 15 singular values. Consequently, the selection of the 30 largest singular values ensures adequate removal of noise components.

In this way, the signal can be reconstructed using only the most

**Table 2**  
Amplitude and Standard Deviation of Resonance Peaks averaged for 200 tests in each group.

Resonance Frequency	Resonance frequency peaks values per group (Mean $\pm$ standard deviation)			
	G100	G75	G50	G25
F1	0.6912 $\pm$ 0.1295	0.7274 $\pm$ 0.1013	0.6436 $\pm$ 0.1004	0.7309 $\pm$ 0.1063
F2	0.6802 $\pm$ 0.1085	0.6299 $\pm$ 0.1121	0.6994 $\pm$ 0.1406	0.7667 $\pm$ 0.1123
F3	0.5845 $\pm$ 0.1404	0.2260 $\pm$ 0.1139	0.4977 $\pm$ 0.0886	0.5394 $\pm$ 0.0938
F4	0.5344 $\pm$ 0.1356	0.2439 $\pm$ 0.1359	0.5196 $\pm$ 0.1708	0.5251 $\pm$ 0.1259
F5	0.6297 $\pm$ 0.1462	0.3291 $\pm$ 0.1291	0.5535 $\pm$ 0.1465	0.5620 $\pm$ 0.1066
F6	0.5319 $\pm$ 0.1386	0.5774 $\pm$ 1247	0.4821 $\pm$ 0.1527	0.4909 $\pm$ 0.1075

**Table 3**  
The mean ( $\bar{x}$ ) and standard deviation ( $\sigma$ ) of characteristic frequencies values (in Hz) averaged across 200 trials for each group.

	f1, Hz	f2, Hz	f3, Hz	f4, Hz	f5, Hz	f6, Hz
G100	299 $\pm$ 1.7	792 $\pm$ 2.8	1586 $\pm$ 10.3	2512 $\pm$ 10	3992 $\pm$ 26.4	5116 $\pm$ 24.1
G75	299 $\pm$ 1.7	792 $\pm$ 2.8	1586 $\pm$ 10.3	2512 $\pm$ 10	3992 $\pm$ 26.4	5116 24.1
G50	300 $\pm$ 2.7	795 $\pm$ 2.8	1596 $\pm$ 13	2519 $\pm$ 11.4	4019 $\pm$ 34.5	5128 $\pm$ 34.9
G25	295 $\pm$ 2.5	792 $\pm$ 2.5	1571 $\pm$ 12	2490 $\pm$ 10	3948 $\pm$ 30.5	4998 $\pm$ 37.7

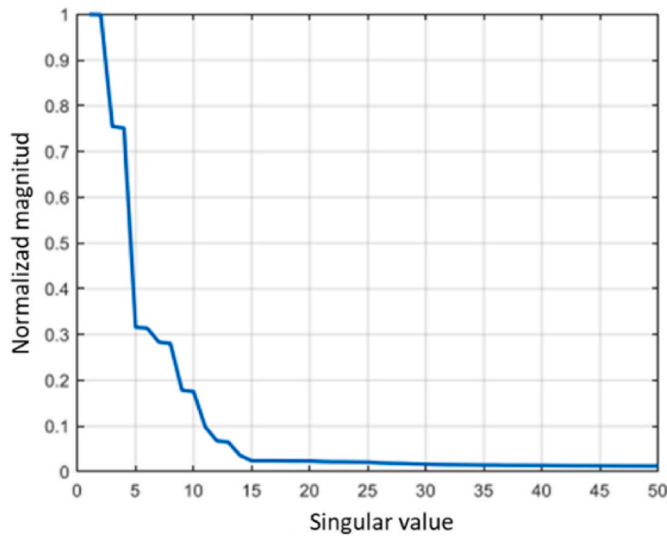


Fig. 4. Singular values distribution of the Hankel matrix.

significant singular values, as the remaining ones are considered associated with noise content. Fig. 5 shows the SPL for the test number 5 for the specimen 2 of the group G100, illustrating the difference between the filtered and original signals, demonstrating the ability of SVD for filtering and reducing noise content while preserving amplitude and natural frequency information.

The filtered signal contains a considerable amount of data that should be reduced in order to use it as input for the classification model [45]. In this regard, the Principal Component Analysis (PCA) technique was employed, where the original N-dimensional dataset is transformed into a new P-dimensional dataset with  $P < N$ . By appropriately selecting the number of principal components to use, a dataset that explains a high percentage of the variance can be obtained. In our work, the first 20 principal components ( $P = 50$ ) were selected since they comprise the 98 % of the variance in the original data [46,47].

3.2.3. Training and testing the classification model

A neural network classification model is a machine learning model that employs a layered structure to assign labels or categories to input data based on certain identifiable features or patterns within that data. As it is trained with more examples, the network becomes more proficient in the classification task. In this work, an ANN model will be trained to classify the specimens according to their adhesion percentage.

The network receives data in a matrix format  $[H_C]$ , which is the result of the preprocessing stage applied to the original signal. This pre-

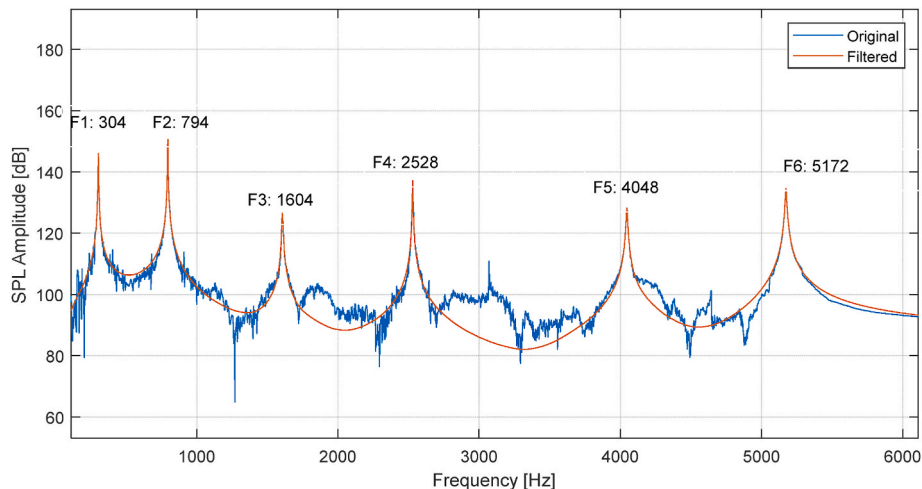


Fig. 5. Original and filtered SPL signal.

processing effectively reduces noise and dimensionality, thereby improving computational efficiency without sacrificing the inherent variability of the data. Each row  $\{H_{C,i}\} = \{H_{C,i}^1, H_{C,i}^2, \dots, H_{C,i}^{50}\}$  in the data matrix  $H_C$  is a vector that represents a particular trial and is associated with a label representing the category corresponding to the adhesion percentage, as indicated in Table 1.

The proposed architecture is a perceptron-type neural network consisting of a three-layer structure. An input layer with 50 neurons corresponding to each of the selected principal components. A hidden layer having 20 fully interconnected neurons (determined experimentally). Finally, an output layer with 4 neurons, one for each output class. This network is depicted in Fig. 6.

Neurons within each layer are governed by distinct activation functions, selected based on the layer's specific role within the overall network architecture. The hidden layer employs the hyperbolic tangent sigmoid (tansig) activation function, which maps input values to the bounded interval  $[-1, 1]$ . The output layer, designed for multi-class classification, utilizes the softmax activation function. Softmax transforms the hidden layer's activations into a categorical probability distribution across the defined output classes. This ensures that the resulting probabilities sum to unity, with each output representing the posterior probability of class membership. The input layer performs no non-linear transformation and simply propagates the input signal to subsequent layers.

The complete dataset was divided into subsets for training and subsequent testing of the model. The cross-validation methodology utilized a leave-one-specimen-out approach. For each fold, data from 20 trials per specimen were obtained from eight selected specimens, yielding a total of 160 trials for training and validation. Data from the remaining, held-out specimen, excluded from the training-validation set, were then used for independent evaluation of the trained model. This leave-one-specimen-out cross-validation was performed iteratively for each of the nine specimens. Consequently, the test data in each iteration were entirely independent of the training data, enabling a robust assessment of the network's generalization performance and its capacity to accurately classify previously unseen trials.

The Levenberg-Marquardt algorithm [48,49] was employed for network training. This algorithm is a classic and powerful choice for training neural networks, particularly in classification problems. As a second-order optimization algorithm, it utilizes information about the second derivative of the error function to guide the optimization process, unlike first-order algorithms (such as standard gradient descent) which only use the first derivative. Second-order algorithms can converge faster and find better local minima. The Levenberg-Marquardt algorithm employs a full-batch approach, calculating the gradient using all training samples in each iteration. Therefore, unlike mini-batch gradient descent, no batch size needs to be explicitly defined. This means that each epoch consists of a single weight update based on the

gradient computed over the entire training dataset. Second-order algorithms leverage information from the Hessian matrix (or an approximation) to guide the optimization process. This Hessian calculation is most computationally efficient when performed using the entire dataset. A learning rate of 0.001 was implemented, with an increase rate of 1.05 and a decrease rate of 0.7. These values resulted in a computationally efficient training process. A learning rate that is too high can cause instability and oscillations, preventing convergence, while a rate that is too low can lead to slow training and the network becoming trapped in a suboptimal local minimum.

The outputs of the network and the previously presented labels are compared to establish the error function. In this study, the cross-entropy loss function was employed to train the neural network for classification. Cross-entropy is a common and effective loss function for classification tasks, particularly when used in conjunction with a softmax output layer. A target error of 0.001 was set as the objective for the loss function during training. The network converges after repeating this procedure a suitable number of times. While a maximum epoch limit of 100 was imposed, the network converged rapidly, reaching the target error within only 14 epochs.

The resulting model is then used to predict the percentage of adhesion of data samples that were not used during the training stage.

## 4. Results and discussion

### 4.1. Frequency data observations

As indicated earlier and illustrated in Fig. 3, there are observed fluctuations in frequency within identical groups. These variations are attributed to the minor differences in mass and dimensions among the 10 specimens. Nonetheless, when comparing across different groups, the discrepancy in frequency values is markedly greater than that observed within the same group. Fig. 7 presents the composite frequency spectrum averaged from the 10 specimens across groups G100 to G25. A notable trend is that an increase in the percentage of adhesive failure correlates with a decrease in frequency values; in other words, there is a downward shift in frequencies as the percentage of adhesive bond diminishes. This trend is consistent across all six identified frequencies, with a more pronounced effect noted at frequencies F5 and F6. Specifically, the mean frequency F1 for group G100, which has 100 % of bonded surface, is at 303 Hz, whereas for group G25, with only 25 %, it drops to 295 Hz. This represents a frequency shift of merely 8 Hz despite a 75 % reduction in adhesion. In contrast, frequency F6 experiences a significant shift from 5190 Hz in group G100 to 4998 Hz in group G25, demonstrating a 192 Hz difference at the sixth frequency due to the same degree of adhesive reduction.

Given the results obtained, it could be thought that the variations in frequencies are due to the mass loss, because the vibration frequencies

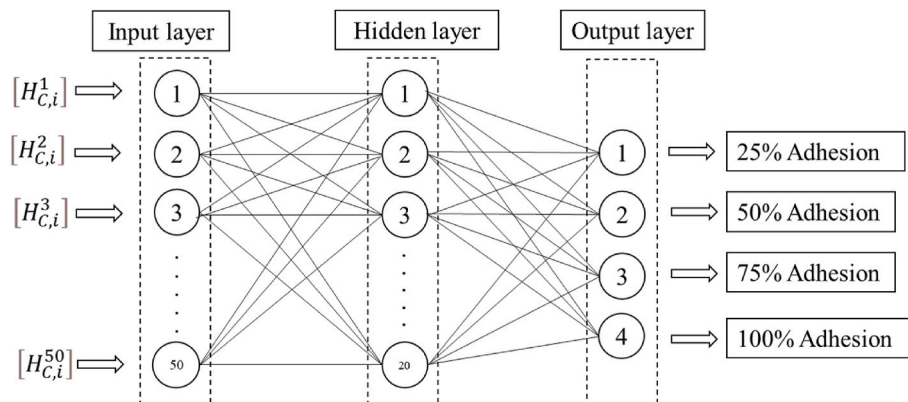


Fig. 6. Architecture of the Artificial Neural Network used for defect detection in bonded joints.

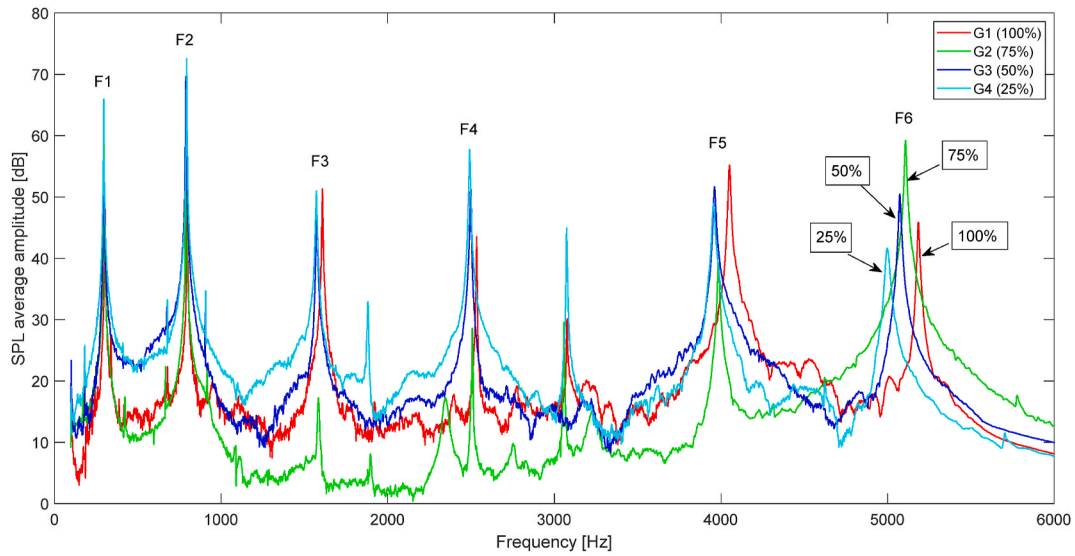


Fig. 7. Average vibration spectra of the four specimen groups: G100 (100 % bonded surface), G75 (75 % bonded), G50 (50 % bonded) and G25 (25 % bonded).

are related to the Young’s Modulus, the dimensions of the specimen and the mass with the frequency proportional to the square root of the rigidity and inversely proportional to the square root of the mass.

The natural vibration frequencies of a freely vibrating structure are greater as the structure loses mass and, in this study, it has been observed that the frequencies are lower, so the changes observed in the samples with a lack of adhesion can only be due to changes in their rigidity. To estimate the effect of mass loss on frequency variation, cured adhesive inserts were manufactured and placed in the gaps of specimens G75 to G25. When testing these specimens with the mass compensated by the insert, a 2 Hz shift is observed at frequencies F4 to F6 towards values lower than those obtained without an insert, while at frequencies F1 to F3 no change is observed. This insignificant frequency shift is consistent when compensating the mass with adhesive inserts between 0.2 and 0.5 g.

Therefore, it can be concluded that the displacement of the natural frequencies towards lower values in the specimens with defects is due to the variation in the rigidity of the structure, since the variation in mass is not significant.

4.2. Descriptive analysis

To assess the statistical significance of the observed differences between the four specimen groups, a p-value analysis was conducted. The results revealed that the differences in frequency values were statistically significant, with a p-value <0.001, indicating that these variations are highly unlikely to have occurred by chance. This indicates that there is less than a 0.1 % probability that the observed differences between groups occurred due to random chance. The use of this stringent threshold ensures robust differentiation among specimen groups based on adhesive bond percentages.

The differentiation of the specimens according to the percentage of bonded surface is primarily due to frequencies F6 and F4. These

frequencies play an important role in predicting the group membership, with the sixth frequency having the greatest discriminatory power.

Utilizing the frequency data from the 40 specimens examined, we derive Fisher’s discriminant functions (Table 4). These functions establish a rule that significantly reduces the likelihood of misclassification errors among the specimens.

Upon applying Fisher’s functions to each of the 40 tested specimens, 38 of them are accurately classified into the correct group, resulting in a 95 % success rate. All specimens from groups G50 and G25 are correctly classified, whereas one specimen from G100 is classified as G75, and one from G75 is classified as G100.

The misclassification observed in two specimens can be attributed to overlapping frequency ranges between these groups at certain frequencies (e.g., F1–F3). This overlap likely arises due to minor variations in specimen dimensions or adhesive properties that were not fully captured by the discriminant functions. Additionally, these specific frequencies exhibit smaller shifts in values compared to F4–F6, which have greater discriminatory power. This limitation highlights the importance of selecting features with high variance across groups for improved classification accuracy.

While a train-test split was not implemented in this study due to the limited dataset size (40 specimens), this approach allowed us to maximize statistical power by using all available data for model development and validation. Dividing the dataset into training and testing subsets would have reduced the sample size available for model training, potentially compromising the reliability of Fisher’s discriminant functions. However, this limits the evaluation of the model’s robustness and generalization capabilities. Future work will address this limitation by incorporating a train-test split or k-fold cross-validation once a larger dataset is available, ensuring a more comprehensive assessment of predictive performance.

Table 4  
Fisher’s linear discriminant functions.

Group (% adhesion)	Fisher Coefficients						
	B <sub>0</sub>	B <sub>1</sub>	B <sub>2</sub>	B <sub>3</sub>	B <sub>4</sub>	B <sub>5</sub>	B <sub>6</sub>
G100 (100 %)	-70713.899	130.994	-15.5	-43.710	108.629	-25.657	2.517
G75 (75 %)	-70183.240	131.705	-14.680	-43.655	108.160	-25.660	2.460
G50 (50 %)	-69984.859	130.031	-11.572	-42.908	106.738	-25.410	2.309
G25 (25 %)	-68858.560	131.034	-8.298	-41.098	105.545	-24.951	1.177

### 4.3. Artificial Neural Network classification

A leave-one-out cross-validation procedure was employed to evaluate the performance of the neural network classification model. This involves using a set of 8 specimens from each group for the training stage and 1 specimen from each group for the testing stage. In total, 640 experimental samples were used for training (4 groups, 8 specimens per group and 20 experimental samples per specimen) and 80 for testing. Using this cross-validation procedure ensures the independence of the data used in the testing stage from that used in the training stage and allowed each specimen to be in the test set once. As a result, 9 ANN models were trained, and the final classification performance was determined by averaging their individual results.

The performance of each model was evaluated using accuracy, precision, and recall, which are commonly used evaluation metrics. Before introducing these metrics, it is important to define four fundamental terms: True Positives (TP), True Negatives (TN), False Positives (FP), and False Negatives (FN).

**TP:** Instances correctly classified as belonging to the positive class.

**TN:** Instances correctly classified as belonging to the negative class.

**FP:** Instances incorrectly classified as belonging to the positive class when they belong to the negative class.

**FN:** Instances incorrectly classified as belonging to the negative class when they belong to the positive class.

Accuracy is determined by dividing the number of correct predictions by the total number of predictions made by the model. It reflects the model's overall ability to correctly classify instances across all predictions. It was calculated as:

$$\text{Accuracy} = \frac{\sum_{i=1}^4 TP_i}{N} \tag{5}$$

Where  $TP_i$  is the number of true positives predictions for the  $i$  class.

A more comprehensive evaluation was complemented by computing the precision and recall values of the classification. Precision is a metric that evaluates the proportion of positive predictions that were truly positive and provides an indication of the network's ability to avoid false positives, meaning predicting a positive class when it is not the actual class. Precision was calculated by dividing the number of correct predictions for the positive class by the total number of positive predictions. That is, for each class  $i$ :

$$\text{Precision}_i = \frac{TP_i}{TP_i + FP_i} \tag{6}$$

Where  $FP_i$  are the number of false positives cases for class  $i$ , that is the number of instances that do not belong to class  $i$  but were incorrectly classified as class  $i$ . Thus, the greater the value of precision, the better the ability of the model to avoid false positives.

On the other hand, Recall measures the model's ability to correctly identify all positive cases in the dataset. It was calculated by dividing the number of correctly classified instances by the total number of instances belonging to the positive class. For each class  $i$ , recall was calculated by:

$$\text{Recall}_i = \frac{TP_i}{TP_i + FN_i} \tag{7}$$

Where  $FN_i$  are the number of false negatives cases for class  $i$ , that is the number of instances that genuinely belong to class  $i$  but were incorrectly classified as another class. Recall is crucial for detecting all positive cases and minimizing false negatives. Thus, the greater the value of Recall, the better the ability of the model to correctly classify the samples.

The performance for each ANN model is summarized in Table 5. Each row displays the accuracy, precision and recall values for a specific model averaged across all classes. Rows also indicate which specimens

**Table 5**

Cross-validation results of the classification process. Each row shows the accuracy, recall and precision values averaged across the testing samples. The final row shows the accuracy, recall and precision values averaged across all models.

ANN model	Training set	Testing set	Accuracy	Recall	Precision
Net 1	Specimens 2 to 9 (S2 to S9)	S1	98.8 %	98.8 %	98.7 %
Net 2	S1 & S3 to S9	S2	92.5 %	94.2 %	92.5 %
Net 3	S1 to S2 & S4 to S9	S3	96.2 %	98.8 %	96.2 %
Net 4	S1 to S3 & S5 to S9	S4	95.0 %	95.2 %	95.0 %
Net 5	S1 to S4 & S6 to S9	S5	98.8 %	98.8 %	98.7 %
Net 6	S1 to S5 & S7 to S9	S6	100 %	100 %	100 %
Net 7	S1 to S6 & S8 to S9	S7	95.0 %	95.2 %	95.0 %
Net 8	S1 to S7 & S9	S8	98.8 %	98.8 %	98.7 %
Net 9	S1 to S8	S9	98.8 %	98.8 %	98.7 %
<b>Average</b>			<b>97.1 %</b>	<b>97.6 %</b>	<b>97.1 %</b>

were used for training and testing, which helps to better understand the cross-validation procedure. The last row presents the overall results of the classification performance, showing the accuracy, precision and recall values averaged across all models. The final classification accuracy was 97.1 %, meaning that 699 out of the 720 samples (180 samples from each class) were correctly classified. Additionally, with a recall average value of 97.6 % and precision average value of 97.0 %, the results confirm that the proposed classification network achieved a satisfactory performance.

Fig. 8 shows the confusion matrix obtained by adding the values of the confusion matrices after evaluating each model. The recall value (last row of the matrix) can be used to indicate the performance of the ANN model to discriminate each group according to the percentage of bonded surface. It is observed that for specimens with 25 % adhesion (G4), all experimental samples were correctly classified (180/180). The rest of the groups have a recall value greater than 94 %, which indicates that the models can discriminate the different groups reliably. On the

		TARGET CLASS				PRECISION
		25% adhesion	50% adhesion	75% adhesion	100% adhesion	
OUTPUT CLASS	25% adhesion	180	0	0	0	100%
	50% adhesion	0	171	2	10	94%
	75% adhesion	0	1	178	0	99%
	100% adhesion	0	8	0	170	96%
RECALL		100%	95%	99%	94%	Accuracy 97.1%

**Fig. 8.** Overall confusion matrix of the cross-validation procedure for evaluating the performance of the ANN classification model.

other hand, the precision values obtained for each group (in all cases greater than 94 %) indicate that the ANN models present a low number of false positives.

## 5. Conclusions

In this study, pre-processed acoustic signals are employed to discriminate different percentages of adhesive failure in aluminum specimens bonded with acrylic adhesive.

As the percentage of adhesive failure in the bonded joints increases, the fundamental vibration frequencies shift towards lower values.

Discriminant analysis was utilized to develop a predictive model to categorize aluminum-acrylic specimens into distinct groups based on the integrity of their adhesive bond. Specifically, the analysis enabled the classification of specimens according to the percentage of bonded area, as inferred from vibrational frequencies obtained through SPL tests. This approach fulfilled two key purposes: first, it enabled the prediction of the adhesive bond condition and the extent of damage based on the analyzed frequencies (it achieved a 95 % accuracy in classifying the manufactured specimens); second, it identified the most impactful independent variables (frequencies) that played a significant role in accurately classifying the test specimens into their respective groups (with frequencies F6 and F4 emerging as the most significant variables in determining the group to which each specimen belongs).

The Artificial Neural Network (ANN) has demonstrated its ability to classify adhesive joints with satisfactory Accuracy, Precision, and Recall values, all achieved with a reasonable computational cost. The classification results obtained using both methods are promising and suggest that further development of the proposed approach is feasible. The authors acknowledge the limitations of this study, particularly the use of artificial flaws created with a Teflon insert. These defects were intended to mimic realistic failure mechanisms in a reproducible and non-destructive manner in order to evaluate the sensitivity and performance of the acoustic NDT techniques in detecting bond integrity issues.

Nevertheless, the results open the door to further research to develop a robust system that automatically detects damage in bonded joints. Given the adaptable nature of pattern recognition algorithms, such systems could be trained to identify a broader range of damage types in adhesive joints. In future experiments, we aim to assess the impact of adhesion failure caused by artificially generated defects introduced through surface contamination and inadequate surface preparation.

## CRedit authorship contribution statement

**Carlos Tais:** Writing – original draft, Validation, Investigation. **Juan M. Fontana:** Writing – review & editing, Validation, Methodology, Data curation. **Leonardo Molisani:** Writing – review & editing, Resources, Methodology, Conceptualization. **Ronald O'Brien:** Methodology, Formal analysis. **Yolanda Ballesteros:** Writing – review & editing, Methodology, Investigation, Conceptualization. **Raquel Caro Carretero:** Visualization, Investigation, Data curation. **Juan C. del Real-Romero:** Supervision, Conceptualization.

## Declaration of competing interest

The authors declare that they have no known competing financial interests or personal relationships that could have appeared to influence the work reported in this paper.

## Data availability

The authors do not have permission to share data.

## References

- [1] da Silva LFM, Ochsner A, Adams RD. Introduction to adhesive bonding technology. In: Handbook of adhesion technology. Springer; 2018.
- [2] Adams R. Bonding adhesive: science, technology and applications. second ed. Woodhead Publishing; 2021.
- [3] Brockmann W, Geiß L, Klingen PL, Schröder B. Adhesive bonding: materials, applications and technology. Wiley-VCH Verlag GmbH & Co. KGaA; 2009.
- [4] Ebnasajjad S. Adhesives technology handbook. second ed. William Andrew; 2009.
- [5] Kandemir MB, Tavşanoğlu T, Seydibeyoğlu MÖ. Investigation of the effect of surface roughness and plasma treatment on adhesively bonded aluminium-polyamide hybrid joints. Int J Adhesion Adhes 2025;139:103964. <https://doi.org/10.1016/j.ijadhadh.2025.103964>.
- [6] Krittanaï C, Honghirun T, Preechasuth B, Nusom Y, Uthaisangasuk V. Mechanical and failure behaviors of adhesively bonded dissimilar materials joints incorporating bio-inspired morphological irregularities. Int J Adhesion Adhes 2025;136:103865. <https://doi.org/10.1016/j.ijadhadh.2024.103865>.
- [7] Ranji S, Lee MC. Study on synthesizing new urethane epoxy adhesives and their adhesive properties on different substrates. Int J Adhesion Adhes 2022;117:103174. <https://doi.org/10.1016/j.ijadhadh.2022.103174>.
- [8] Papon E. Adhesive families. In: Handbook of adhesion technology. Springer; 2018.
- [9] Del Real JC, Ballesteros Y, Chamochin R, Abenojar J, Molisani L. Influence of surface preparation on the fracture behavior of acrylic adhesive/CFRP composite joints. J Adhes 2011;87:366–81. <https://doi.org/10.1080/00218464.2011.562114>.
- [10] Huang JP, Lean J. Advances in acrylic structural adhesives. In: Advances in structural adhesive bonding. Woodhead Publishing; 2023. p. 69–101.
- [11] Righettini RF. Structural acrylics. In: Surfaces, chemistry and applications, adhesion science and engineering series. Amsterdam: Elsevier; 2002. p. 823–46.
- [12] Adams RD. Non destructive testing. In: Handbook of adhesion technology. Springer; 2018.
- [13] Michaloudaki M, Lehmann E, Kosteas D. Neutron imaging as a tool for the non-destructive evaluation of adhesive joints in aluminium. Int J Adhesion Adhes 2005; 25:257–67. <https://doi.org/10.1016/j.ijadhadh.2004.06.006>.
- [14] Zhuang Y, Kopsaftopoulos F, Dugnani R, Chang F-K. Integrity monitoring of adhesively bonded joints via an electromechanical impedance-based approach. Struct Health Monit 2018;17:1031–45. <https://doi.org/10.1177/1475921717732331>.
- [15] Maeva E, Severina I, Bondarenko S, Chapman G, O'Neill B, Severin F, Maev RGR. Acoustical methods for the investigation of adhesively bonded structures: a review. Can J Phys 2004;82:981–1025. <https://doi.org/10.1139/p04-056>.
- [16] Jasiūnienė E, Yilmaz B, Smagulova D, Bhat GA, Cicėnas V, Zukauskas E, Maziška L. Non-destructive evaluation of the quality of adhesive joints using ultrasound, X-ray, and feature-based data fusion. Appl Sci 2022;12:12930. <https://doi.org/10.3390/app122412930>.
- [17] Li W, Liang Y, Liu Y. Failure load prediction and optimisation for adhesively bonded joints enabled by deep learning and fruit fly optimisation. Adv Eng Inform 2022;54. <https://doi.org/10.1016/j.aei.2022.101817>.
- [18] Ramalho GMF, M. Lopes A, Carbas RJC, Da Silva LFM. Identifying weak adhesion in single-lap joints using lamb wave data and artificial intelligence algorithms. Appl Sci 2023;13:2642. <https://doi.org/10.3390/app13042642>.
- [19] Sommer D, Haufe A, Middendorf P. A machine learning material model for structural adhesives in finite element analysis. Int J Adhesion Adhes 2022;117:103160. <https://doi.org/10.1016/j.ijadhadh.2022.103160>.
- [20] Chiang LH, Kotanchek ME, Kordon AK. Fault diagnosis based on Fisher discriminant analysis and support vector machines. Comput Chem Eng 2004;28:1389–401. <https://doi.org/10.1016/j.compchemeng.2003.10.002>.
- [21] Chiang LH, Russell EL. Fault detection and diagnosis in industrial systems. New York: Springer-Verlag; 2001.
- [22] Wu P, Lou S, Zhang X, He J, Liu Y, Gao J. Data-driven fault diagnosis using deep canonical variate analysis and Fisher discriminant analysis. IEEE Trans Ind Inf 2021;17:3324–34. <https://doi.org/10.1109/TII.2020.3030179>.
- [23] Malinowski PH, Ecault R, Wandowski T, Ostachowicz WM. Evaluation of adhesively bonded composites by nondestructive techniques. In: Kundu T, editor. Presented at the SPIE smart structures and materials + nondestructive evaluation and health monitoring; 2017. 101700B. <https://doi.org/10.1117/12.2259852>. Portland, Oregon, United States.
- [24] Sharkawy A-N. Principle of neural network and its main types: review. J Adv Appl Comput Math 2020;7:8–19. <https://doi.org/10.15377/2409-5761.2020.07.2>.
- [25] Jain LC, Lim CP, Balasubramaniam P, Seera M. A review of online learning in supervised neural networks. Neural Comput Appl 2014;25:491–509.
- [26] Zhao X, Wang L, Zhang Y, Han X, Deveci M, Parmar M. A review of convolutional neural networks in computer vision. Artif Intell Rev 2024;57:99. <https://doi.org/10.1007/s10462-024-10721-6>.
- [27] Otter DW, Medina JR, Kalita JK. A survey of the usages of deep learning for natural language processing. IEEE Transact Neural Networks Learn Syst 2021;32:604–24. <https://doi.org/10.1109/TNNLS.2020.2979670>.
- [28] Tama BA, Vania M, Lee S, Lim S. Recent advances in the application of deep learning for fault diagnosis of rotating machinery using vibration signals. Artif Intell Rev 2023;56:4667–709. <https://doi.org/10.1007/s10462-022-10293-3>.
- [29] Chulkov AO, Vavilov VP, Shagdyrov BI, Kladov DYu. Automated detection and characterization of defects in composite-metal structures by using active infrared thermography. J Nondestruct Eval 2023;42:20. <https://doi.org/10.1007/s10921-023-00929-x>.
- [30] Duan Y, Liu S, Hu C, Hu J, Zhang H, Yan Y, Tao N, Zhang C, Maldague X, Fang Q, Ibarra-Castaneda C, Chen D, Li X, Meng J. Automated defect classification in

- infrared thermography based on a neural network. *NDT E Int* 2019;107:102147. <https://doi.org/10.1016/j.ndteint.2019.102147>.
- [31] He C, Yang S, Liu Z, Wu B. Damage localization and quantification of truss structure based on electromechanical impedance technique and neural network. *Shock Vib* 2014;1–9. <https://doi.org/10.1155/2014/727404>.
- [32] Birecikli B, Karaman ÖA, Çelebi SB, Turgut A. Failure load prediction of adhesively bonded GFRP composite joints using artificial neural networks. *J Mech Sci Technol* 2020;34:4631–40. <https://doi.org/10.1007/s12206-020-1021-7>.
- [33] Gajewski J, Golewski P, Sadowski T. The use of neural networks in the analysis of dual adhesive single lap joints subjected to uniaxial tensile test. *Materials* 2021;14:419. <https://doi.org/10.3390/ma14020419>.
- [34] Samaitis V, Yilmaz B, Jasiuniene E. Adhesive bond quality classification using machine learning algorithms based on ultrasonic pulse-echo immersion data. *J Sound Vib* 2023;546:117457. <https://doi.org/10.1016/j.jsv.2022.117457>.
- [35] Smagulova D, Samaitis V, Jasiuniene E. Machine learning based approach for automatic defect detection and classification in adhesive joints. *NDT E Int* 2024;148:103221. <https://doi.org/10.1016/j.ndteint.2024.103221>.
- [36] American Society For Testing Materials. ASTM E 1876-2006 standard test method for dynamic young's Modulus, shear Modulus, and Poisson's ratio by impulse excitation of vibration. 2006.
- [37] American National Standards Institute. ANSI S1.1-2013, acoustical terminology. 2013.
- [38] International Standards Organization. ISO 389-1:2017. Acoustics — reference zero for the calibration of audiometric equipment — Part 1: reference sound pressure levels. 2017.
- [39] Hair JF, Black WC, Babin BJ, Anderson RE. *Multivariate data analysis*. eighth ed., eighth ed. 2018. Cengage Learning.
- [40] McLachlan JG. *Discriminant analysis and statistical pattern recognition*, Wiley series in probability and statistics. Wiley; 1992.
- [41] Rencher AC, Christensen WF. *Methods of multivariate analysis*, Wiley series in probability and statistics. Wiley; 2012.
- [42] Verma RK. A study on the applications of discriminant analysis. *Int J Phys Appl* 2025;7:16–9. <https://doi.org/10.33545/26647575.2025.v7.i1a.121>.
- [43] Fahey SO, Wicks AL. Noise sources in mechanical measurements. *Exp Tech* 2000;24:40–3. <https://doi.org/10.1111/j.1747-1567.2000.tb02271.x>.
- [44] Sanliturk KY, Cakar O. Noise elimination from measured frequency response functions. *Mech Syst Signal Process* 2005;19:615–31.
- [45] Jolliffe IT, Cadima J. Principal component analysis: a review and recent developments. *Philos Trans R Soc Math Phys Eng Sci* 2016;374:20150202. <https://doi.org/10.1098/rsta.2015.0202>.
- [46] O'Brien RJ, Fontana JM, Ponso N, Molisani L. A pattern recognition system based on acoustic signals for fault detection on composite materials. *Eur J Mech - ASolids* 2017;64:1–10. <https://doi.org/10.1016/j.euromechsol.2017.01.007>.
- [47] Ponso N, Molisani L, Zapico A, Real JCD, Ballesteros Y. Eliminación de ruidos de señales acústicas usando Descomposición de Valores Singulares y Análisis de Componentes Principales. *Mecánica Comput* 2012;XXXI:4013–27.
- [48] Levenberg K. A method for the solution of certain non-linear problems in least squares. *Q Appl Math* 1944;2:164–8. <https://doi.org/10.1090/qam/10666>.
- [49] Marquardt DW. An algorithm for least-squares estimation of nonlinear parameters. *J Soc Ind Appl Math* 1963;11:431–41. <https://doi.org/10.1137/0111030>.